Published in final edited form as:
Chem Res Toxicol. 2009 March 16; 22(3): 433–445. doi:10.1021/tx8002752.

Comparative Analysis of Gene Expression Changes Mediated by Individual Constituents of Hemozoin

Alexandra C. Schrimpe and **David W. Wright***
Department of Chemistry, Vanderbilt University, Nashville, Tennessee 37235

Abstract

Plasmodium protozoa, the source of malarial infections, catabolize large quantities of hemoglobin during an intra-erythrocytic phase. During this process, free heme is detoxified through biomineralization into an insoluble heme aggregate, hemozoin (Hz). In its native state, Hz is associated with a variety of lipid peroxidation products including 4-hydroxy-2-nonenal (HNE). In the present study, gene expression profiles were used to compare responses to two of the individual components of Hz in a model macrophage cell line. LPS-stimulated RAW 264.7 cells were exposed to HNE and the synthetic form of Hz, β-hematin (BH), for 6 or 24 h. Microarray analysis identified alterations in gene expression induced by exposure to HNE and opsonized BH (fold change ≥1.8, *p*-value ≤0.01). Patterns of gene expression were compared to changes induced by an opsonized control latex bead challenge in LPS-stimulated cells and revealed that the BH response was predominantly phagocytic. Ingenuity Pathway Analysis demonstrated that HNE mediated a short term oxidative stress response and had a prolonged effect on the expression of genes associated with categories of 'Cell Cycle', 'Cellular Assembly and Organization', 'DNA Replication, Recombination, and Repair', and 'Cellular Development'. Comparisons of expression changes caused by BH and HNE with those observed during malarial infection suggest that BH and HNE are involved in inflammatory response modulation, altered NF-κB signal transduction, extracellular matrix (ECM) degradation, and dyserythropoiesis. HNE exposure led to several significant steady-state expression changes including repressed chemokine (C-C motif) ligand 5 (*Ccl5*) indicative of dyserythropoiesis, and a severe matrix metalloproteinase 9 (*Mmp9*)/tissue inhibitor of metalloproteinase 1 (*Timp1*) imbalance in favor of ECM proteolysis.

Introduction

Parasitic resistance to drugs, vector resistance to insecticides, and climatic and environmental changes, have caused a global resurgence of the *Plasmodium* infection, malaria (1). Progress towards the treatment and prevention of infection is hindered by the complex parasite lifecycle and host-pathogen interactions. Many of the hallmarks of malaria

*To whom correspondence should be addressed. Tel: (615) 322-2636. Fax: (615) 322-1234. david.w.wright@vanderbilt.edu.

Supporting Information Available: Representative SEM image of BH and histogram showing the length distribution of particles (S1) and flow cytometric analyses of latex bead phagocytosis (S2), BH phagocytosis (S3), and potential cell death mediated by HNE (S4). Selected genes that are associated with (A) specific genes or gene products correlated to malarial infection or (B) genes that are classified under specific over-expressed biological processes in malaria models that are modulated ≥ 1.8 fold by 35 μM HNE or 0.1 mg/mL BH at 6 or 24 h are shown in Supplementary Tables 1–8. This information is available free of charge via the Internet at http://pubs.acs.org.

are associated with the rupture of parasitized erythrocytes, release of cellular and parasite debris into the vasculature, and subsequent immune response. Although immune activity is essential for protective immunity, a modulated response likely contributes to malaria pathogenesis (2). Accumulating evidence suggests that many adverse effects are caused by endogenous toxins generated during interactions of parasite-derived species with host tissues (3). Consequently, the interplay between various parasite-derived species, including hemozoin (Hz), and the host immune system is of extreme interest.

Hz is a heme detoxification biomineral formed during the intraerythrocytic parasite stage as a result of the high concentration of free heme released during hemoglobin catabolism. Structurally, the biomineral is an aggregate of hydrogen bonded five-coordinate ferric protoporphyrin IX [Fe(III)PPIX] dimers, joined by reciprocating monodentate carboxylate linkages between the central iron of one monomer and a propionic acid side chain of the other (4). In its native state, Hz is coated by an array of proteins, nucleic acids, host- and parasite-derived lipids (5), and racemic lipid peroxidation products (6). Notably, the level of the secondary oxidation product 4-hydroxy-2-nonenal (HNE) measured in Hz-laden monocytes (7) is the highest intracellular HNE concentration in any biological system observed to date (8).

At schizogony, it is estimated that cellular debris, including 200 μmol of particulate Hz, is released into the circulation of a *P. falciparum*-infected patient (9) initiating an innate immune response. Hz has been shown to perturb the expression of cytokines (9–11) and impair both re-phagocytosis (12) and phorbol ester mediated oxidative burst (13). Given the activity of native Hz against an activated immune response, it is of interest to understand the effects of individual Hz components on macrophage function. Recently, the immunomodulatory activity of native Hz was modeled using constitutive components in a cell culture system. Membrane lipids from erythrocyte ghosts were incubated with BH, and RAW 264.7 macrophage-like cells subsequently exposed. These cells demonstrated impaired PMA-activated NADPH oxidase and LPS-stimulated inducible nitric oxide synthase (iNOS) activities. Upon treatment with either BH- or ghost-supernatant alone, no inhibition was observed indicating that lipid peroxidation products generated during reactions between BH and ghost membranes were responsible for the effects.

The known cellular responses to several lipid peroxidation components of Hz suggests possible involvement in malaria pathophysiology (6, 14). The current study aims to dissect the components of Hz in a model system and explore potential roles of key players involved in disrupting the programmed function of the triggered immune response during infection. Since the effects of the individual components of Hz remain largely unexplored in the context of malaria, a microarray approach was used to explore gene expression changes in activated cells. Given the unquestionable reactivity of HNE (8, 15, 16), and ability of the heme moiety to mediate lipid peroxidation (17–19), HNE and BH were targeted as the native Hz components. Gene expression patterns were analyzed in the context of biological processes to examine the downstream effects of both specific and non-specific damage, and comparisons were made with cellular alterations that are observed during malarial infection.

Experimental Procedures

β-hematin Synthesis and Characterization

BH was synthesized as previously described (20, 21) using purified hemin chloride (Fluka). Exhaustive washings in MeOH, 0.1 M NaHCO3 (pH 9.0), and DMSO removed excess free heme and small aggregates. Formation was confirmed by powder X-ray diffraction (Scintag X1 h/h automated powder difractometer with a copper target, a Peltier-cooled solid-state detector and a zero-background silica (510) sample support) and FTIR spectroscopy (ATI Mattson Genesis Series). BH was suspended in ethanol, sonicated, applied to a polished aluminum specimen mount, and dried at 25 °C overnight. The sample was sputter-coated with gold for 20 s and imaged using a Hitachi S4200 scanning electron microscope at 1.0 kV accelerating voltage. Particles were determined to have an average length of 0.9 ± 0.3 μM (Supporting Information Figure 1).

Cell Culture and Treatment

Murine macrophage-like RAW 264.7 cells (American Type Culture Collection) were cultured under standard incubation conditions (37 °C, 5% CO_2) and grown in RPMI supplemented with 5% FBS (Atlanta Biologicals) and 1μg/mL P/S (Cellgro MediaTech). Cells were untreated or treated with 35 μM HNE (EMD Biosciences), 0.1 mg/mL serum-opsonized BH, or serum-opsonized latex bead (0.1μm, 10 μL of 0.05% per 1×10^6 cells), and immediately stimulated with LPS (1 μg/mL). Opsonization was performed as previously described (22).

RNA Isolation and Expression Analysis

Microarray and qRT-PCR analyses were performed by the Vanderbilt Microarray Shared Resource. Total RNA was isolated using the Versagene RNA purification and DNase treatment kits, following manufacturer's recommendations. Three biological replicates per sample were analyzed for quality (Agilent 2100 Bioanalyzer, Agilent Technologies). One (1) μg of Total RNA (30 ng mRNA) was used to generate First Strand cDNA using the NanoAmp RT-IVT labeling kit according to manufacturer's protocol. Following first strand synthesis, second strand synthesis was completed. The resulting cDNA was then purified using an ABI kit provided column and the entire reaction was used in an IVT reaction to generate cRNA or DIG labeled cRNA. cRNA was purified using a kit provided column, assessed for quality on an Agilent Bioanalyzer, and reverse transcribed to make ss cDNA. Samples prepared from 6 h incubations were fragmented, labeled with terminal deoxy transferase with biotin, hybridized to an Affymetrix mouse gene 1.0ST arrays per manufacturer's protocol, and detected with Streptavidin-Phycoerythrin. Samples obtained from 24 h incubations were fragmented, hybridized to an ABI mouse genome survey microarray per manufacturer's protocol, and detected with the addition of the chemiluminescence reaction substrate. Expression values were quantile normalized and filtered (S/N >3 and flag value <5000, ABI arrays). Partek 6.4 and GeneSpring GX 7.3.1 software were used to determine statistically significant differentially expressed genes from probes altered by ≤ or ≥ 1.8-fold (0.01 p-value cutoff, Benjamini-Hochberg multiple testing correction) in treated stimulated cells (experimental) relative to stimulated cells (control). In accordance with MIAME procedure, microarray data have been submitted to the NCBI

Gene Expression Omnibus and can be found under series number GSE13281. Ingenuity Pathways Analysis was used for gene expression analysis (Ingenuity Systems®, www.ingenuity.com).

Quantitative real-time reverse transcription polymerase chain reaction (qRT-PCR) was used to validate the expression levels of several genes identified as differentially expressed (quadruplicate measurements of three biological replicates per sample). cDNA was reverse-transcribed from 0.5 μg of total RNA using random hexamer primers and Superscript II Reverse Transcriptase (Invitrogen). Reactions were purified using Qiagen's PCR Purification Kit following the manufacturer's protocol. Following RT, all assays were performed with Applied Biosystems TaqMan FAM labeled 20× probes (Table 1). Ywhaz was chosen as the endogenous control based on results obtained from an Applied Biosystems mouse endogenous control array. cDNA amplification was performed using TaqMan 2× Universal PCR Master Mix (Applied Biosystems) and standard Taqman cycling conditions were used as specified by the manufacturer. Cycling and data collection were performed using the Applied Biosystems 7900 HT instrument and analysis performed using SDS software to calculate Ct values for each detector. Ct values were processed based on the comparative Ct method.

ELISA

Cells (4×10^6 cells/well in 6 well plates) were plated and incubated for 24 h. The cells were washed once with DPBS and treated in triplicate with LPS (1 μg/mL) or HNE (35 μM) + LPS (1 μg/mL). Cell culture medium was collected at 0 or 24 h, and GCSF and MMP9 protein levels were determined using commercial ELISA reagents (R&D Systems) according to manufacturer's protocol.

Flow Cytometric Analysis

Phagocytosis and cell death assays were performed on a BD LSRII flow cytometer. At least 10,000 events per sample were collected for the determination of cell populations using FACSDiva v6.1.1. After the indicated time post serum opsonized-BH or -latex bead treatment, cells were washed with DPBS and incubated at 37 °C for 15 minutes in CellStripper non-enzymatic cell dissociation buffer (Cellgro MediaTech). Potential HNE-mediated cell death was determined by the Vybrant Apoptosis Assay Kit II (Invitrogen) according to the manufacturer's instructions. Briefly, cells were harvested, resuspended in assay buffer, and stained with Alexa Fluor 488 conjugated Annexin V and propidium iodide (PI). Sample analysis was performed using FloJo v8.8.2 (Treestar).

Results

Analysis of gene expression changes in BH- or HNE-treated, LPS-stimulated RAW 264.7 cells

LPS stimulated macrophage-like RAW 264.7 cells were exposed to 0.1 mg/mL BH or 35 μM HNE for 6 or 24 h. The concentrations of BH and HNE were chosen based on reported estimates of Hz (100 μM) in brain capillaries of malaria victims (23) and HNE (40 μM) levels in Hz-fed monocytes (7). Phagocytosis of opsonized-latex beads and -BH was

examined by flow cytometry. Latex bead fluorescence was detected in 86 % and 99 % of the gated parent population at 6 and 24 h, respectively, demonstrating the level of phagocytosis (Supporting Information Figure 2). Accumulation of Hz within monocytes has been shown to, apart from an increase in depolarized side scatter, considerably increase conventional side scatter (24). In BH treated cells, phagocytosis of the total population was indicated by a marked increase in conventional side scatter mean fluorescence versus control cells (Supporting Information Figure 3). It was previously shown by confocal microscopy that opsonized BH was ingested by RAW 264.7 cells and localized within the phagolysosome (21). Given the possibility of HNE to induce cell death, the effect of 35 μM HNE on RAW 264.7 cell death was investigated. Changes in viable, apoptotic, and dead cell populations were measured by flow cytometry 24 h after treatment of LPS stimulated cells (Supporting Information Figure 4). Evaluation of cells with apoptosis- and necrosis-specific stains demonstrated that HNE only altered the percentage of apoptotic cells by 3.4 % relative to stimulated cells. The population of necrotic cells was unchanged regardless of HNE treatment. These values demonstrate that 24 h incubation of 35 μM HNE is well tolerated by RAW 264.7 cells.

Statistically significant ($p \leq 0.01$) gene expression changes (fold change ≥1.8 relative to control), where expression is considered a measurement of the RNA abundance at the time of isolation, were identified by microarray analysis. Within each treatment category, differentially expressed genes were sorted into lists based on the direction of regulation and compared to identify common changes relative to stimulated cells (Figure 1a–d). In order to identify expression changes dependent on interactions of BH rather than those due to phagocytosis, differentially expressed genes were controlled by a corresponding particulate latex bead challenge. Six hours post-challenge, there were no significant expression changes mediated by latex bead phagocytosis, and only a small group (i.e., 39 genes) altered by BH phagocytosis. Steady-state mRNA levels (24 h) demonstrate that nearly 70% of the genes differentially expressed by BH are in common with the ‘inert’ latex bead control, indicating that the response to BH is predominantly phagocytic. Consequently, phagocytosis-related genes were identified and disregarded for remaining analyses. The number of genes differentially expressed by HNE or BH treatment indicates the degree of perturbation by each of the native Hz-associated components. HNE treatment altered a significantly larger group of genes than BH treatment, suggesting a more serious impact on cellular function.

Ingenuity Pathway Analysis (IPA) was used to perform a functional analysis of each dataset. IPA functional analysis ranks molecular and cellular functions according to Fischer’s Exact Test p-value. Those categories exhibiting $p < 0.001$ are shown in Table 2 for both BH and HNE treatment datasets at 6 and 24 h timepoints. The magnitude of response to either BH or HNE treatment is evident from the number of significantly affected biological processes identified by IPA. At 6 h, both BH and HNE affect a diverse group of functions including ‘Cell Signaling’ and ‘Small Molecule Biochemistry’ among others. By 24 h, the cellular response to BH is minimal. Given that BH does not impair microbicidal functions, is sensitive to microbicidal agents, and is degraded upon phagocytosis in RAW 264.7 cells (21), it was not surprising to find that the steady-state response to BH was modest. The degree of perturbation by HNE at 24 h complements literature observations regarding its extensive reactivity with cellular nucleophiles (15, 16, 25–29). Expression changes mediated

by BH and HNE indicate differential cellular responses to both treatments as a function of time. There is, however, some overlap in the early and late response to HNE, primarily associated with ‘Stress Response’, ‘Immune Response’, and ‘Gene Expression’ (listed within Table 3).

Differential gene expression in the context of malaria pathogenesis

Microarray data from this study were compared to two groups of genes. The first group consists of specific genes or gene products that are associated with human (30, 31) or murine (32, 33) models of malarial infection, and/or BH or Hz (9, 10) exposure. The second group includes genes that are classified with specific biological processes that are over-expressed in a murine *P. yoelii* model (33) and/or naturally-acquired *P. falciparum* infections (34) (e.g., cell-cell signaling, defense response, immune response, inflammatory response, and signal transduction). Complete lists of differentially expressed genes altered by either HNE or BH treatment that fall within these categories are listed in Supporting Information Tables 1–9.

Validation of microarray results

qRT-PCR was used to confirm several genes susceptible to differential regulation by HNE and BH at 6 h and 24 h (Table 1). Analysis was focused on selected genes implicated in the host response to malaria. The results shown in Figure 2 are expressed as fold change relative to stimulated cells (control). At 6 h, RT-PCR confirmed that HNE repressed the expression of chemokine (C-C motif) ligand 2 (*Ccl2*), colony stimulating factor 3 (granulocyte) (*Csf3*), tissue inhibitor of metalloproteinase 1 (*Timp1*), matrix metalloproteinase 9 (*Mmp9*), *Csf2*, interleukin (Il) 1 alpha (*Il1a*) and 1 beta (*Il1b*), and BH down-regulated colony stimulating factor 2 (granulocyte-macrophage) (*Csf2*) relative to stimulated cells. At 24 h, HNE enhanced expression of *Mmp9*, nuclear factor of kappa light polypeptide gene enhancer in B-cells inhibitor, epsilon (*Nfkbie*), inhibitor of kappaB kinase epsilon (*Ikbke*), tumor necrosis factor (*Tnf*), and *Csf3*. Concurrently, *Timp1* and chemokine (C-C motif) ligand 5 (*Ccl5*) genes were repressed. RT-PCR analyses of BH-treated cells at 24 h confirmed *Il1a* stimulation and FBJ osteosarcoma oncogene (*Fos*) suppression. These results are consistent with the microarray data. ELISA studies showed that HNE treatment induced MMP9 and CSF3 translation and release relative to stimulated cells (Figure 3).

Discussion

It has been suggested that the immunological activity resulting from native Hz may not be due to the biomineral itself, but to a toxin that is presented on its surface (35). Lipid peroxidation products have been implicated as potential non-specific Hz toxins. Heme compounds are effective mediators of non-enzymatic lipid oxidation, supporting the premise that these products arise from the oxidation of lipids by Hz. Further, purified Hz and BH have been shown to drive the oxidation of arachidonic acid to racemic mixtures of HETEs, HODEs, (17, 19) and HNE (18). In a native state, these molecules are adsorbed to the surface of the biomineral and introduced into the cell during phagocytosis of Hz.

Several groups have reported conflicting results concerning the effects of the biomineral in both in vitro and in vivo systems (36–38). As Hz is complex in nature, the state of the material must be well-defined in order to identify which components are responsible for a given immune response. Native Hz has been isolated from parasitized erythrocytes and gently washed to remove cellular debris but left with a lipid coat adsorbed onto the hydrophobic porphyrin plane (12). Purified Hz refers to native Hz whose lipid coat has been removed (39, 40). Finally, BH has been prepared and purified from hemin, and is consequently devoid of all biologically-derived components (20, 37, 41, 42). Many of the reported differences in cellular response are likely attributable to the source of the biomineral (native vs. synthetic), purification procedure, and the method of macrophage activation (e.g., LPS, interferon-γ (IFN-γ), LPS+IFN-γ, or PMA). In order to facilitate consistent interpretation of the response to individual Hz components in the current study, the impact of BH and HNE was investigated on LPS-activated macrophage-like cells.

Given the relationship between high levels of Hz observed in victims, severity of infection, and disruption of macrophage function, microarray technology was used to profile expression changes mediated by two defined Hz-derived components, BH and HNE, in LPS-stimulated macrophage-like RAW 264.7 cells. Expression changes are calculated relative to LPS-stimulated cells to measure the response to each hemozoin component in an activated cell.

Stress response

Regulation of antioxidant response element (ARE) gene expression is controlled by the transcription factor NRF2, whose activity is suppressed through the formation of a complex with its inhibitor Keap1. Disruption of NRF2/Keap1 complex liberates NRF2, allowing its nuclear translocation and subsequent activation of ARE-dependent gene expression. Consistent with previous findings in a variety of cell types treated with HNE (8, 15), a potent “oxidative stress response mediated by Nrf2” was observed at both 6 h and 24 h following HNE treatment, suggesting an effort to reduce cellular damage (Table 3). Expression of genes encoding phase I and II metabolizing enzymes and antioxidant response proteins was significantly enhanced by HNE. Activation of a stress response is consistent with an increase of *Prdx1* in the spleens of *P. berghei* infected mice (32) and *Sod2* and *Hmox1* in both the blood of acute pediatric malaria victims (30) and Hz-loaded placental tissue (31). A common stress response is heme oxygenase (decycling) 1 (*Hmox1*) induction. In the current study *Hmox1* expression is induced by both HNE and BH at 6 h. This observation is in agreement with up-regulated *Hmox1* expression in mouse peritoneal macrophages (PM) treated with BH (43).

Cell cycle checkpoint signaling

The present data indicate a broad ‘DNA replication, Recombination, and Repair’ response to HNE at 6 and 24 h. Early expression of several genes associated with checkpoint control is repressed. By 24 h, however, a dramatic DNA damage response including the induction of a number of genes associated with G1/S cell cycle checkpoint regulation was observed (Figure 4 and Table 3). Since HNE can form adducts with deoxyguanosine residues (44), activation of cell cycle checkpoint signaling genes suggests an effort to ameliorate DNA

injury. The presence of damaged DNA is consistent with enhanced expression of excision repair and mismatch repair genes at 24 h. Notably, increased *ATM* and *RAD23A* expression has also been identified in whole blood of *P. falciparum* infected children (30).

Macrophage activation

An exacerbated inflammatory response is assumed to play a significant role in malaria pathogenesis. In an effort to uncover the basis of the inflammatory activity, Hz has been examined as a contributing agent (9, 10). This microarray analysis demonstrates that BH had a modest effect on the induction of immune response genes at 6 h and 24 (Table 4). HNE treatment, however, drastically repressed expression of immune/inflammatory response genes (Figure 4b) and interferon-signaling and -regulated genes at 6h. By 24 h, the response was reversed and the induction of a large group of immune/inflammatory response genes was identified (Table 3). Notably, this change in response over time may explain the often contradictory interpretation of Hz and immune cell interactions reported in the literature (9, 10, 12, 36–38, 45).

A number of specific studies probing the inflammatory response to malaria are consistent with the observed HNE-mediated gene expression changes: murine kidneys infected with *P. berghei* display increased expression of TNF-α (46), and *P. falciparum* exposed CHO cells exhibit increased levels of TNF-α, G-CSF, and TGF-β (47). Several individual expression changes also correspond with responses observed in microarray analyses of genuine or experimental malaria. For example, messages for *LY96, CD14* and *C5R1* in whole blood of pediatric victims (30) *CD2, C5R1* and *IL10RA* in placental malaria (31), and *Cd2* in a *P. yoelii* infected mice (33) are consistent with enhanced expression by HNE in the current analysis.

Although HNE and BH augment the expression of genes involved in mounting an immune response, they repress the expression of a number of genes central to a cell's antigen presenting ability (Tables 3 and 4). The present study identified significant ($p < 0.05$) steady-state repression of antigen major histocompatibility complex (MHC) class II-associated genes in both HNE- and BH-treated cells. Notably, Hz loading has been implicated as a factor contributing to both impaired monocyte MHC class II antigen presentation (22) and defective dendritic cell function (14, 48). The ability of HNE, and to a lesser extent BH, to suppress MHC II expression implies two Hz components involved in the defective responses. Furthermore, elevated levels of TGF-β and PGE_2 are associated with T-cell inhibition (49). HNE enhanced the expression of genes encoding *Tgfb* and *Ptges* and may contribute to the impaired T-cell activity observed upon Hz phagocytosis.

NF-κB signaling

The LPS mediated pathway to produce nitric oxide (NO) is well characterized and entails NF-κB signal transduction. In quiescent cells, NF-κB is sequestered by inhibitory proteins (IκB) in the cytoplasm. Upon activation, IκB kinase (IKK) phosphorylates IκB, triggering its polyubiquitination and subsequent degradation. Once NF-κB is liberated from IκB, NF-κB translocates to the nucleus and regulates gene expression, including iNOS.

It has been shown that serum withdrawal in RAW 264.7 cells results in the activation of NF-κB, expression of iNOS, and synthesis of NO. However, serum withdrawal-mediated IκB phosphorylation and downstream signaling was abolished in HNE treated cells (50). In accord with this data, HNE prevented NO production in LPS-stimulated RAW 264.7 cells (21). HNE has been shown to covalently adduct to IKK, inhibiting kinase activity thus preventing the phosphorylation of IκB (28). As a result, IκB degradation and NF-κB translocation are impaired.

Unlike HNE, there are a wide range of observations regarding the effects of Hz and BH on iNOS activity and NO synthesis. For example, both BH and purified Hz do not inhibit IFN-γ mediated NO in B10R murine macrophage cells (40). Similarly, RAW 264.7 cells stimulated by LPS and loaded with BH exhibit normal NO levels (21). In contrast, LPS-mediated NO production is reduced in BH treated murine PM cells (43). Skorokhod et al. found that levels of NO are not impaired in several murine phagocytic cell lines after crude Hz or BH loading, but determined that human monocytes are unable to produce NO when stimulated with either LPS or IFN-γ (51). Further, native Hz decreases NO in LPS or IFN-γ stimulated murine PM suggesting that a non-heme moiety component is responsible for the dysfunction (52). This varied group of results demonstrates the need for careful extrapolation of NO production data based on cell type, stimulatory molecule, and the state of the Hz preparation.

In the present study, HNE, and not BH, had an impact on NF-κB related gene expression (Table 3). Early changes in expression indicate repression of the NF-κB pathway (down-regulated *Cd40, Nfkb1*, and *Nfkbiz* levels) by HNE. However, at 24 h, IKK (i.e., *Ikbke*) and IκB (*Nfkbia, Nfkbie*) expression is enhanced. Notably, transcript abundance does not necessarily correlate with protein level or kinase activity. In accord with the HNE studies mentioned above, IKK expression may be increased because the available enzyme is inactivated by HNE. Due to the numerous gene expression modulations mediated by HNE, it seems probable that most are a result of downstream effects of HNE interactions. The increase of IKK expression, however, may be a direct response to dysregulated kinase activity.

ECM degradation

A current hypothesis is that expression changes of ECM genes may have direct involvement in malaria pathogenesis, particularly in cases of cerebral malaria (CM). CM is a severe complication of *P. falciparum* infection that is characterized by adherence of parasitized RBC to the cerebral microvasculature. Analysis of the brain vessels from CM mouse models reveals Hz accumulation not only within parasites, but also free and within phagocytic cells (53). Further, examination of the cortex of postmortem CM victims shows slate-gray discoloration, commonly attributed to Hz deposition (54). Blood brain barrier (BBB) destruction is a major factor associated with CM (55). Matrix metalloproteinases (MMPs), secreted enzymes involved in ECM remodeling, are able to degrade basal lamina leading to BBB damage (56). Interestingly, Hz increases the transcription, translation, and activity of MMP9 in monocytes (57). Activation of *MMP9* is also observed during *P. falciparum*

infection (30) and may contribute to the disruption of endothelial basement membranes and extravasation of blood cells (57).

The activity of MMP9 is controlled by its cognate inhibitor, TIMP1. HNE exposure initially repressed *Mmp9* expression, however, by 24 h the level of mRNA was significantly increased. Notably, both 6 h and steady-state mRNA levels of HNE treated samples indicate severely impaired *Timp1* expression (−2000-fold at 24 h by qRT-PCR). Taken together, *Mmp9* induction coupled with *Timp1* repression indicates a steady state MMP9/TIMP1 imbalance that may lead to increased proteolysis of the ECM (Table 3) (57). *Mmp9* expression can be regulated through a variety of signaling cascades including NF-κB, p38 MAPK, and ERK1/2 pathways (58–60). Given that HNE abrogates NF-κB mediated iNOS expression in both LPS stimulated- and serum deprived-RAW 264.7 cells, *Mmp9* up-regulation in the present study is not a result of NF-κB activation (21, 50).

Active MMP9 is capable of pro-TNF-α cleavage which releases the active cytokine and promotes *Mmp9* expression (61). Thus, the increased expression of *Tnf* discussed previously may enhance a positive feedback cycle in this study. Importantly, analyses of postmortem brain tissue of CM victims identified elevated TNF mRNA and protein (62), and immunostaining studies identified significant cerebrum, brainstem, and cerebellar localization (63).

CM victims possess several traits including obstructed microvascular flow, attributable to the sequestration of blood cells including parasitized RBC and leukocytes (64). Intercellular adhesion molecule 1 (ICAM1), one of the most important receptors involved in cytoadherence (65), is upregulated in naturally-acquired malaria and may contribute to ECM degradation (65, 66). In the current study, HNE up-regulated *Icam1* expression at 6 and 24 h (Table 3). Through cell adhesion, ICAM1 aids ECM binding and may trigger macrophage accumulation and localized MMP9 activity.

Dyserythropoiesis

The specific mechanism(s) leading to malarial anemia have not been clearly defined, but several factors including dyserythropoiesis are thought to play a role (67). Casals-Pascual et al. provide evidence correlating dyserythropoiesis with Hz (68). Further, HNE and the supernatant of native Hz-fed monocytes have both been shown to dose-dependently inhibit erythroid-progenitor growth in culture (69). Repressed CCL5 has been correlated with dyserythropoiesis and may be a contributing factor (70). Interestingly, CM victims, which have been found with significant Hz accumulation in their brains (54), exhibit decreased levels of CCL5 (71). The significant repression of *Ccl5* expression by HNE at 24 h suggests a potential role in dyserythropoiesis. Moreover, impaired expression of two upstream regulators of *Ccl5*, namely *Traf3* and *Tsc22d3*, may be directly involved in *Ccl5* repression in the current study (Table 3).

Conclusion

The host immune response to malarial infection is multifactorial, including complex innate and adaptive immune responses to the parasites, composite native Hz, Hz-derived lipid

peroxidation products, and other cellular debris. Not unexpectedly, countless interactions between an array of malaria toxins and host cells result in adverse biological effects, prompting a reductionist examination of such complex systems. In the current study, gene expression analysis of HNE-treated cells supports some role for HNE in malaria pathogenesis. A wide range of substantive modulations occurred in activated cells following HNE treatment at both 6 and 24 h. The early response predominantly involves an oxidative stress activity that involves induction of ARE and glutathione metabolism genes. Steady state gene expression changes are associated with a variety of documented malaria responses such as macrophage activation, immune and inflammatory responses, NF-κB signal transduction, ECM degradation, and dyserythropoiesis. The modest, primarily phagocytic, response to BH supports the hypothesis that Hz predominantly functions as a vehicle to generate and introduce toxic mediators (e.g., HNE, hydroxylated fatty acids) that are closely associated with the biomineral into phagocytic cells (35). Further, the gene expression changes induced by HNE may be illustrative of other reactive lipid oxidation products generated by Hz. Although valuable for exploring the interactions between Hz components and immune active cells, it must be kept in perspective that there are limitations to using any model system. It is possible that stimulation antagonizes expression changes mediated by BH or HNE. However, activated immune cells are physiologically relevant in the pathology of malaria. Future studies will be aimed at comparing BH- and HNE-mediated gene expression changes with those resulting from other biologically active Hz-associated components, and confirming expression changes in primary human macrophages and monocytes.

Supplementary Material

Refer to Web version on PubMed Central for supplementary material.

Acknowledgments

Financial support for this work was provided by NIH (NIAID) grant R03AI060827. The Vanderbilt Microarray Shared Resource is supported by the Vanderbilt Ingram Cancer Center (P30 CA68485), the Vanderbilt Digestive Disease Center (P30 DK58404) and the Vanderbilt Vision Center (P30 EY08126). The VMC Flow Cytometry Shared Resource is supported by the Vanderbilt Ingram Cancer Center (P30 CA68485) and the Vanderbilt Digestive Disease Research Center (DK058404). We thank M. F. Richards for editorial assistance.

Abbreviations

Hz	hemozoin
HNE	4-hydroxy-2-nonenal
BH	β-hematin
ECM	extracellular matrix
HETE	hydroxyeicosatetraenoic acid
HODE	hydroxyoctadecadienoic acid
RBC	red blood cell

LPS	lipopolysaccharide
PMA	phorbol-12-myristate-13-acetate
iNOS	inducible nitric oxide synthase
IPA	Ingenuity Pathway Analysis
qRT-PCR	quantitative real-time reverse transcription polymerase chain reaction
MHC	major histocompatibility complex
NO	nitric oxide
PM	peritoneal macrophage
CM	cerebral malaria
BBB	blood brain barrier

References

1. Greenwood B, Mutabingwa T. Malaria in 2002. Nature. 2002; 415:670–672. [PubMed: 11832954]
2. Urquhart AD. Putative pathophysiological interactions of cytokines and phagocytic cells in severe human falciparum malaria. Clin. Infect. Dis. 1994; 19:117–131. [PubMed: 7948512]
3. Boutlis CS, Yeo TW, Anstey NM. Malaria tolerance - for whom the cell tolls? Trends Parasitol. 2006; 22:371–377. [PubMed: 16784889]
4. Pagola S, Stephens PW, Bohle DS, Kosar AD, Madsen SK. The structure of malaria pigment β-haematin. Nature. 2000; 404:307–310. [PubMed: 10749217]
5. Goldie P, Roth EF Jr, Oppenheim J, Vanderberg JP. Biochemical characterization of *Plasmodium falciparum* hemozoin. Am. J. Trop. Med. Hyg. 1990; 43:584–596. [PubMed: 2267961]
6. Schwarzer E, Kuhn H, Valente E, Arese P. Malaria-parasitized erythrocytes and hemozoin nonenzymatically generate large amounts of hydroxy fatty acids that inhibit monocyte functions. Blood. 2003; 101:722–728. [PubMed: 12393662]
7. Schwarzer E, Muller O, Arese P, Siems WG, Grune T. Increased Levels of 4-hydroxynonenal in human monocytes fed with malarial pigment hemozoin. FEBS Lett. 1996; 338:119–122. [PubMed: 8690068]
8. Poli G, Schaur RJ, Siems WG, Leonarduzzi G. 4-Hydroxynonenal: A membrane lipid oxidation product of medicinal interest. Medicinal Research Reviews. 2008; 28:569–631. [PubMed: 18058921]
9. Sherry BA, Alava G, Tracey KJ, Martiney J, Cerami A, Slater AF. Malaria-specific metabolite hemozoin mediates the release of several potent endogenous pyrogens (TNF, MIP-1 alpha, and MIP-1 beta) in vitro, and altered thermoregulation in vivo. J Inflamm. 1995; 45:85–96. [PubMed: 7583361]
10. Prada J, Malinowski J, Muller S, Bienzle U, Kremsner PG. Hemozoin differentially modulates the production of interleukin 6 and tumor necrosis factor in murine malaria. Eur. Cytokine Network. 1995; 6:109–112.
11. Ochiel DO, Awandare GA, Keller CC, Hittner JB, Kremsner PG, Weinberg JB, Perkins DJ. Differential regulation of B-chemokines in children with Plasmodium falciparum malaria. Infect. Immun. 2005; 73:4190–4197. [PubMed: 15972509]
12. Schwarzer E, Turrini F, Ulliers D, Giribaldi G, Ginsburg H, Arese P. Impairment of macrophage functions after ingestion of Plasmodium falciparum-infected erythrocytes or isolated malarial pigment. J. Exp. Med. 1992; 176:1033–1041. [PubMed: 1402649]

13. Schwarzer E, Arese P. Phagocytosis of malarial pigment hemozoin inhibits NADPH-oxidase activity in human monocyte-derived macrophages. Biochim. Biophys. Acta. 1996; 1316:169–175. [PubMed: 8781535]
14. Skorokhod OA, Alessio M, Mordmuller B, Arese P, Schwarzer E. Hemozoin (malarial pigment) inhibits differentiation and maturation of human monocyte-derived dendritic cells: a peroxisome proliferator-activated receptor-γ-mediated effect. J. Immunol. 2004; 173:4066–4074. [PubMed: 15356156]
15. West JD, Marnett LJ. Alterations in gene expression induced by the lipid peroxidation product, 4-hydroxy-2-nonenal. Chem. Res. Toxicol. 2005; 18:1642–1653. [PubMed: 16300372]
16. Weigel AL, Handa JT, Hjelmeland LM. Microarray analysis of H2O2-, HNE, or tBH-treated Arpe-19 cells. Free Radical Biol. Med. 2002; 33:1419–1432. [PubMed: 12419474]
17. Green MD, Xiao L, Lal AA. Formation of hydroxyeicosatetraenoic acids from hemozoin-catalyzed oxidation of arachidonic acid. Mol. Biochem. Parasitol. 1996; 83:183–188. [PubMed: 9027751]
18. Miller CM, Carney CK, Schrimpe AC, Wright DW. B-hematin (hemozoin) mediated decomposition of polyunsaturated fatty acids to 4-hydroxy-2-nonenal. Inorg. Chem. 2005; 44:2134–2136. [PubMed: 15792445]
19. Carter MD, Reese Harry S, Wright DW. Identification of hydroxyeicosatetraenoic acid components of schistosomal hemozoin. Biochem. Biophys. Res. Commun. 2007; 363:867–872. [PubMed: 17904531]
20. Bohle DS, Helms JB. Synthesis of β-hematin by dehydrohalogenation of hemin. Biochem. Biophys. Res. Commun. 1993; 193:504–508. [PubMed: 8512553]
21. Carney CK, Schrimpe AC, Halfpenny K, Harry RS, Miller CM, Broncel M, Sewell SL, Schaff JE, Deol R, Carter MD, Wright DW. The basis of the immunomodulatory activity of malaria pigment (hemozoin). J. Biol. Inorg. Chem. 2006; 11:917–929. [PubMed: 16868743]
22. Schwarzer E, Alessio M, Ulliers D, Arese P. Phagocytosis of the malarial pigment, hemozoin, impairs expression of major histocompatibility complex class II antigen, CD54, and CD11c in human monocytes. Infect. Immun. 1998; 66:1601–1606. [PubMed: 9529087]
23. Huy NT, Trang DTX, Kariu T, Sasai M, Saida K, Harada S, Kamei K. Leukocyte activation by malarial pigment. Parasit. Int. 2006; 55:75–81.
24. Krämer B, Grobusch MP, Suttorp N, Neukammer J, Rinneberg H. Relative frequency of malaria pigment-carrying monocytes of nonimmune and semi-immune patients from flow cytometric depolarized side scatter. Cytometry. 2001; 45:133–140. [PubMed: 11590625]
25. Chen J, Henderson GI, Freeman GL. Role of 4-Hydroxynonenal in modification of cytochrome C oxidase in ischemia/reperfused rat heart. J. Mol. Cell. Cardiol. 2001; 33:1919–1927. [PubMed: 11708837]
26. Schaur RJ. Basic aspects of the biochemical reactivity of 4-hydroxynonenal. Mol. Aspects Med. 2003; 24:149–159. [PubMed: 12892992]
27. Crabb JW, O'Neil J, Miyagi M, West K, Hoff HF. Hydroxynonenal inactivates cathepsin B by forming Michael adducts with active site residues. Protein Sci. 2002; 11:831–840. [PubMed: 11910026]
28. Ji C, Kozak KR, Marnett LJ. Ikappa B kinase, a molecular target for inhibition by 4-hydroxy-2-nonenal. J. Biol. Chem. 2001; 276:18223–18228. [PubMed: 11359792]
29. Szweda LI, Uchida K, Tsai L, Stadtman ER. Inactivation of glucose-6-phosphate dehydrogenase by 4-hydroxy-2-nonenal. Selective modification of an active-site lysine. J. Biol. Chem. 1993; 268:3342–3347. [PubMed: 8429010]
30. Griffiths MJ, Mohammed JS, Popper SJ, Hemingway CA, Kortok MM, Wathen A, Rockett KA, Mott R, Levin M, Newton CR, Marsh K, Relman DA, Kwiatkowski DP. Genomewide analysis of the host response to malaria in Kenyan children. J. Infect. Dis. 2005; 191:1599–1611. [PubMed: 15838786]
31. Muehlenbachs A, Fried M, Lachowitzer J, Mutabingwa TK, Duffy PE. Genome-wide expression analysis of placental malaria reveals features of lymphoid neogenesis during chronic infection. J. Immunol. 2007; 179:557–565. [PubMed: 17579077]
32. Sexton AC, Good RT, Hansen DS, D'Ombrain MC, Buckingham L, Simpson K, Schofield L. Transcriptional profiling reveals suppressed erythropoiesis, up-regulated glycolysis, and

interferon-associated responses in murine malaria. J. Infect. Dis. 2004; 189:1245–1256. [PubMed: 15031794]

33. Schaecher K, Kumar S, Yadava A, Vahey M, Ockenhouse CF. Genome-wide expression profiling in malaria infection reveals transcriptional changes associated with lethal and nonlethal outcomes. Infect. Immun. 2005; 73:6091–6100. [PubMed: 16113330]
34. Ockenhouse CF, Hu W-c, Kester KE, Cummings JF, Stewart A, Heppner DG, Jedlicka AE, Scott AL, Wolfe ND, Vahey M, Burke DS. Common and divergent immune response signaling pathways discovered in peripheral blood mononuclear cell gene expression patterns in presymptomatic and clinically apparent malaria. Infect. Immun. 2006; 74:5561–5573. [PubMed: 16988231]
35. Nguyen PH, Day N, Pram TD, Ferguson DJ, White NJ. Intraleucocytic malaria pigment and prognosis in severe malaria. Trans. R. Soc. Trop. Med. Hyg. 1995; 89:200–204. [PubMed: 7778149]
36. Jaramillo M, Plante I, Ouellet N, Vandal K, Tessier PA, Olivier M. Hemozoin-inducible proinflammatory events in vivo: potential role in malaria infection. J. Immunol. 2004; 172:3101–3110. [PubMed: 14978116]
37. Taramelli D, Basilico N, Pagani E, Grande R, Monti D, Ghione M, Olliaro P. The heme moiety of malaria pigment (β-hematin) mediates the inhibition of nitric oxide and tumor necrosis factor-α production by lipopolysaccharide-stimulated macrophages. Exp. Parasitol. 1995; 81:501–511. [PubMed: 8542991]
38. Jaramillo M, Godbout M, Olivier M. Hemozoin induces macrophage chemokine expression through oxidative stress-dependent and -independent mechanisms. J. Immunol. 2005; 174:475–484. [PubMed: 15611273]
39. Biswas S, Karmarkar MG, Sharma YD. Antibodies detected against Plasmodium falciparum haemozoin with inhibitory properties to cytokine production. FEMS Microbiol. Lett. 2001; 194:175–179. [PubMed: 11164304]
40. Jaramillo M, Gowda DC, Radzioch D, Olivier M. Hemozoin increases IFN-gamma-inducible macrophage nitric oxide generation through extracellular signal-regulated kinase- and NF-kappa B-dependent pathways. J. Immunol. 2003; 171:4243–4253. [PubMed: 14530348]
41. Slater AF, Swiggard WJ, Orton BR, Flitter WD, Goldberg DE, Cerami A, Henderson GB. An iron-carboxylate bond links the heme units of malaria pigment. Proc Natl Acad Sci USA. 1991; 88:325–329. [PubMed: 1988933]
42. Blauer G, Akkawi M. Investigations of B- and β-Hematin. J. Inorg. Biochem. 1997; 66:145–152. [PubMed: 9112763]
43. Taramelli D, Recalcati S, Basilico N, Olliaro P, Cairo G. Macrophage preconditioning with synthetic malaria pigment reduces cytokine production via heme iron-dependent oxidative stress. Lab. Invest. 2000; 80:1781–1788. [PubMed: 11140691]
44. Douki T, Odin F, Caillat S, Favier A, Cadet J. Predominance of the 1,N2-propano 2'-deoxyguanosine adduct among 4-hydroxy-2-nonenal-induced DNA lesions. Free Radical Biol. Med. 2004; 37:62–70. [PubMed: 15183195]
45. Pichyangkul S, Saengkrai P, Webster HK. Plasmodium falciparum pigment induces monocytes to release high levels of tumor necrosis factor-α and interleukin-1β. Am. J. Trop. Med. Hyg. 1994; 51:430–435. [PubMed: 7943569]
46. Sinniah R, Rui-Mei L, Kara A. Up-regulation of cytokines in glomerulonephritis associated with murine malaria infection. Int. J. Exp. Pathol. 1999; 80:87–95. [PubMed: 10469263]
47. Wahlgren M, Abrams JS, Fernandez V, Bejarano MT, Azuma M, Torii M, Aikawa M, Howard RJ. Adhesion of Plasmodium falciparum-infected erythrocytes to human cells and secretion of cytokines (IL-1-beta, IL-1RA, IL-6, IL-8, IL-10, TGF beta, TNF alpha, G-CSF, GM-CSF. Scand. J. Immunol. 1995; 42:626–636. [PubMed: 8552986]
48. Millington OR, Lorenzo CD, Phillips S, Garside P, Brewer JM. Suppression of adaptive immunity to heterologous antigens during Plasmodium infection through hemozoin-induced failure of dendritic cell function. J. Biol. 2006; 5:5. [PubMed: 16611373]

49. Ocaña-Morgner C, Wong, Kurt A, Lega F, Dotor J, Borras-Cuesta F, Rodriguez A. Role of TGF-beta and PGE2 in T cell responses during Plasmodium yoelii infection. Eur. J. Immunol. 2007; 37:1562–1574. [PubMed: 17474154]
50. Liu W, Kato M, Itoigawa M, Murakami H, Yajima M, Wu J, Ishikawa N, Nakashima I. Distinct involvement of NF-κB and p38 mitogen-activated protein kinase pathways in serum deprivation-mediated stimulation of inducible nitric oxide synthase and its inhibition by 4-hydroxynonenal. J. Cell. Biochem. 2001; 83:271–280. [PubMed: 11573244]
51. Skorokhod OA, Schwarzer E, Ceretto M, Arese P. Malarial pigment haemozoin, IFN-gamma, TNF-alpha, IL-1beta and LPS do not stimulate expression of inducible nitric oxide synthase and production of nitric oxide in immuno-purified human monocytes. Malar. J. 2007; 6:73–80. [PubMed: 17543124]
52. Prada J, Malinowsky J, Muller S, Bienzle U, Kremsner PG. Effects of Plasmodium vinckei hemozoin on the production of oxygen radicals and nitrogen oxides in murine macrophages. Am. J. Trop. Med. Hyg. 1996; 54:620–624. [PubMed: 8686781]
53. Sullivan AD, Ittarat I, Meshnick SR. Patterns of haemozoin accumulation in tissue. Parasitology. 1996; 112:285–294. [PubMed: 8728992]
54. Newton CR, Taylor TE, Whitten RO. Pathophysiology of fatal falciparum malaria in African children. Am. J. Trop. Med. Hyg. 1998; 58:673–683. [PubMed: 9598460]
55. Adams S, Brown H, Turner G. Breaking down the blood-brain barrier: signaling a path to cerebral malaria? Trends Parasitol. 2002; 18:360–366. [PubMed: 12377286]
56. Mandal M, Mandal A, Das S, Chakraborti T, Chakraborti S. Clinical implications of matrix metalloproteinases. Mol. Cell. Biochem. 2003; 252:305–329. [PubMed: 14577606]
57. Prato M, Giribaldi G, Polimeni M, Gallo V, Arese P. Phagocytosis of hemozoin enhances matrix metalloproteinase-9 activity and TNF-alpha production in human monocytes: role of matrix metalloproteinases in the pathogenesis of falciparum malaria. J Immunol. 2005; 175:6436–6442. [PubMed: 16272296]
58. Woo C-H, Lim J-H, Kim J-H. Lipopolysaccharide induces matrix metalloproteinase-9 expression via a mitochondrial reactive oxygen species-p38 kinase-activator protein-1 pathway in RAW 264.7 Cells. J Immunol. 2004; 173:6973–6980. [PubMed: 15557194]
59. Lai W-C, Zhou M, Shankavaram U, Peng G, Wahl LM. Differential regulation of lipopolysaccharide-induced monocyte matrix metalloproteinase (MMP)-1 and MMP-9 by p38 and extracellular signal-regulated kinase 1/2 mitogen-activated protein kinases. J Immunol. 2003; 170:6244–6249. [PubMed: 12794156]
60. Rhee JW, Lee KW, Kim D, Lee Y, Jeon OH, Kwon HJ, Kim DS. NF-kappaB-dependent regulation of matrix metalloproteinase-9 gene expression by lipopolysaccharide in a macrophage cell line RAW 264.7. J Biochem Mol Biol. 2007; 40:88–94. [PubMed: 17244487]
61. Gearing AJH, Beckett P, Christodoulou M, Churchill M, Clements J, Davidson AH, Drummond AH, Galloway WA, Gilbert R, Gordon JL, Leber TM, Mangan M, Miller K, Nayee P, Owen K, Patel S, Thomas W, Wells G, Wood LM, Woolley K. Processing of tumour necrosis factor-α precursor by metalloproteinases. Nature. 1994; 370:555–557. [PubMed: 8052310]
62. Brown H, Turner G, Rogerson S, Tembo M, Mwenechanya J, Molyneux M, Taylor T. Cytokine expression in the brain in human cerebral malaria. The Journal of Infectious Diseases. 1999; 180:1742–1746. [PubMed: 10515846]
63. Armah H, Wiredu EK, Dodoo AK, Adjei AA, Tettey Y, Gyasi R. Cytokines and adhesion molecules expression in the brain in human cerebral malaria. Int. J. Environ. Res. Public Health. 2005; 2:123–131. [PubMed: 16705810]
64. Wassmer SC, Combes V, Candal FJ, Juhan-Vague I, Grau GE. Platelets potentiate brain endothelial alterations induced by Plasmodium falciparum. Infect. Immun. 2006; 74:645–653. [PubMed: 16369021]
65. Turner GDH, Morrison H, Jones M, Davis TME, Looareesuwan S, Buley ID, Gatter KC, Newbold CI, Pukritayakamee S, Nagachinta B, White NJ, Berendt AR. An immunohistochemical study of the pathology of fatal malaria: evidence for widespread endothelial activation and a potential role for intercellular adhesion molecule-1 in cerebral sequestration. Am. J. Pathol. 1994; 145:1057–1069. [PubMed: 7526692]

66. Silamut K, Phu NH, Whitty C, Turner GDH, Louwrier K, Mai NTH, Simpson JA, Hien TT, White NJ. A quantitative analysis of the microvascular sequestration of malaria parasites in the human brain. Am. J. Pathol. 1999; 155:395–410. [PubMed: 10433933]

67. Mohan and Stevenson. Dyserythropoiesis and severe anaemia associated with malaria correlate with deficient interleukin-12 production. Br. J. Haematol. 1998; 103:942–949. [PubMed: 9886304]

68. Casals-Pascual C, Kai O, Cheung JOP, Williams S, Lowe B, Nyanoti M, Williams TN, Maitland K, Molyneux M, Newton CRJC, Peshu N, Watt SM, Roberts DJ. Suppression of erythropoiesis in malarial anemia is associated with hemozoin in vitro and in vivo. Blood. 2006; 108:2569–2577. [PubMed: 16804108]

69. Giribaldi G, Ulliers D, Schwarzer E, Roberts I, Piacibello W, Arese P. Hemozoin- and 4-hydroxynonenal-mediated inhibition of erythropoiesis. Possible role in malarial dyserythropoiesis and anemia. Haematologica. 2004; 89:492–493. [PubMed: 15075084]

70. Were T, Hittner JB, Ouma C, Otieno RO, Orago AS, Ong'echa JM, Vulule JM, Keller CC, Perkins DJ. Suppression of RANTES in children with Plasmodium falciparum malaria. Haematologica. 2006; 91:1396–1399. [PubMed: 17018392]

71. John CC, Opika-Opoka R, Byarugaba J, Idro R, Boivin MJ. Low levels of RANTES are associated with mortality in children with cerebral malaria. J. Infect. Dis. 2006; 194:837–845. [PubMed: 16941352]

72. Lovegrove FE, Pena-Castillo L, Mohammad N, Liles C, Hughes TR, Kain KC. Simultaneous host and parasite expression profiling identifies tissue-specific transcriptional programs associated with susceptibility or resistance to experimental cerebral malaria. BMC Genomics. 2006; 7:295–311. [PubMed: 17118208]

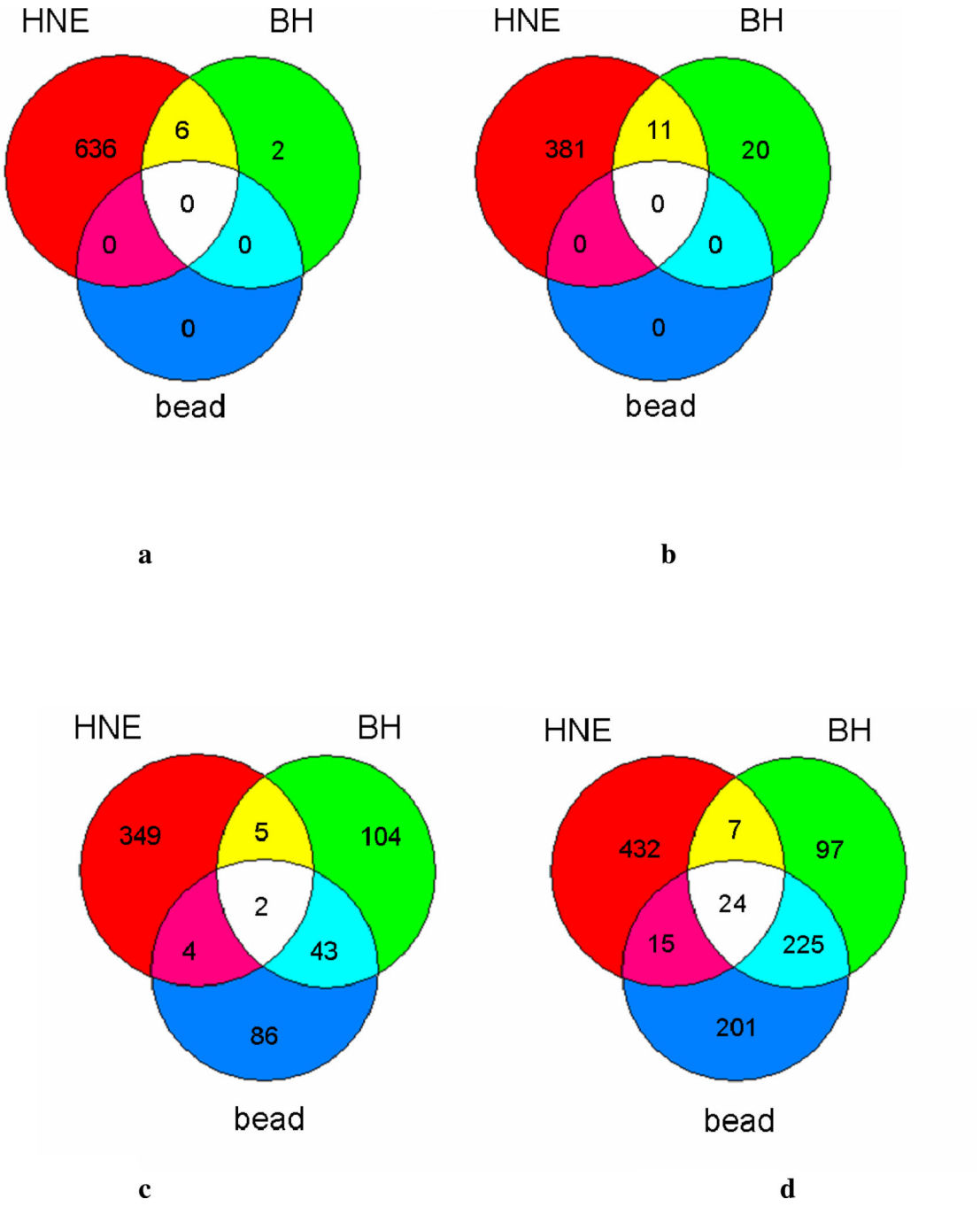

Figure 1.

Overlapping genes with significant differential expression mediated by BH and HNE. Venn diagrams show the intersection of genes that were altered by 0.1 mg/mL BH with those altered by either latex bead or 35 μM HNE treatment. Numbers represent statistically significant ($p \leq 0.01$) genes up- or down-regulated ≥1.8-fold relative to LPS stimulated cells at 24 h. (a) down-regulated genes identified at 6 h, (b) up-regulated genes identified at 6 h, (c) down-regulated genes identified at 24 h, (d) up-regulated genes identified at 24 h.

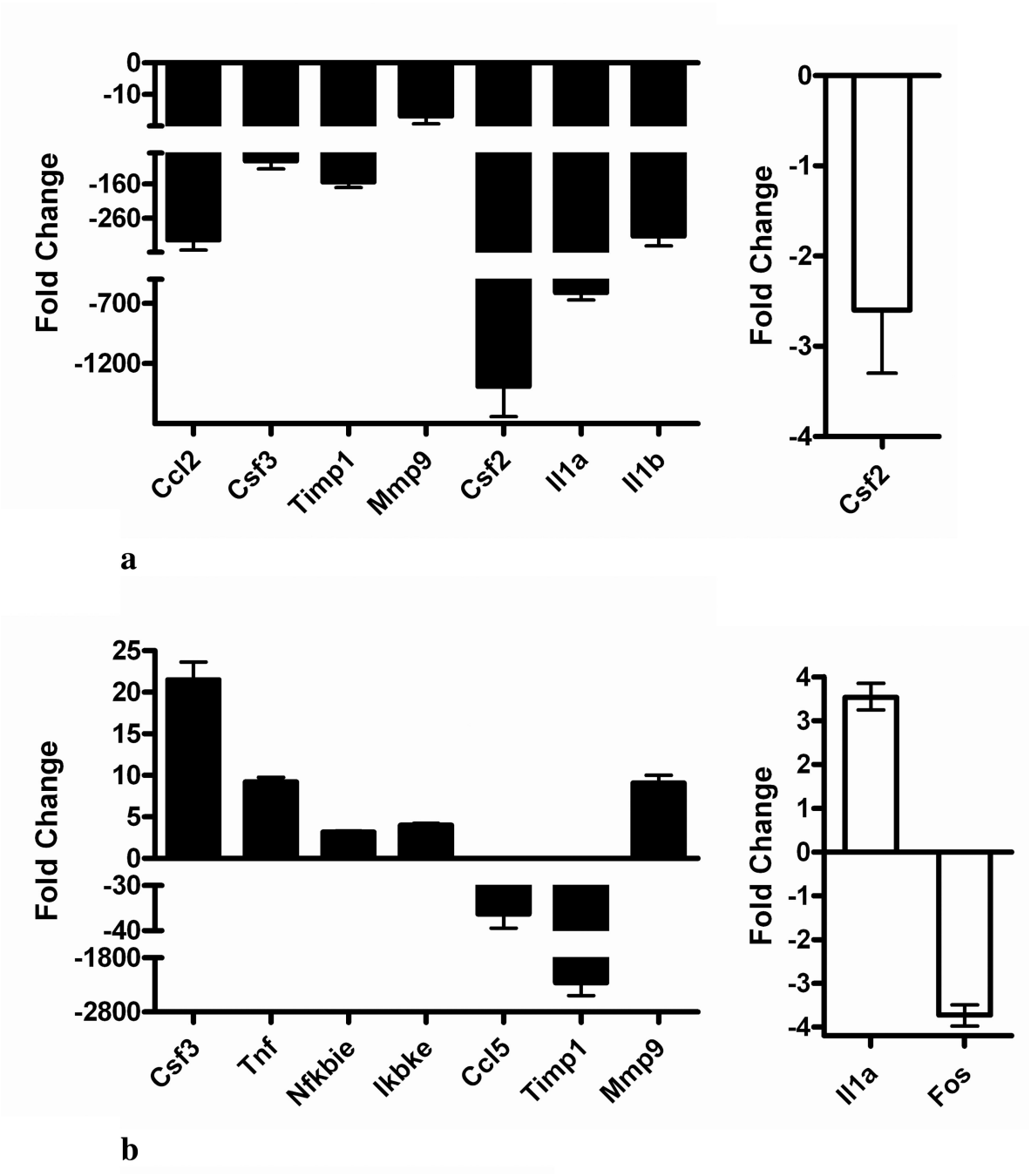

Figure 2.

Quantitative real-time RT-PCR validation of microarray results. RAW 264.7 cells were stimulated with 0.1 μg/mL LPS and untreated or treated (A) for 6 h or (B) for 24 h with either 35 μM HNE (black bars) or 0.1 mg/mL BH (white bars). Fold-changes (treated, stimulated cells relative to stimulated controls) are shown ($\bar{X} \pm$ 99% confidence interval for quadruplicate measurements of n = 3 biological replicates). Abbreviations: chemokine (C-C motif) ligand (*Ccl*); colony stimulating factor (*Csf*); tissue inhibitor of metalloproteinase 1 (*Timp1*); matrix metalloproteinase 9 (*Mmp9*); interleukin 1 (*Il1*); tumor necrosis factor

(*Tnf*); nuclear factor of kappa light polypeptide gene enhancer in B-cells inhibitor, epsilon (*Nfkbie*); inhibitor of kappaB kinase, epsilon (*Ikbke*); and FBJ osteosarcoma oncogene (*Fos*).

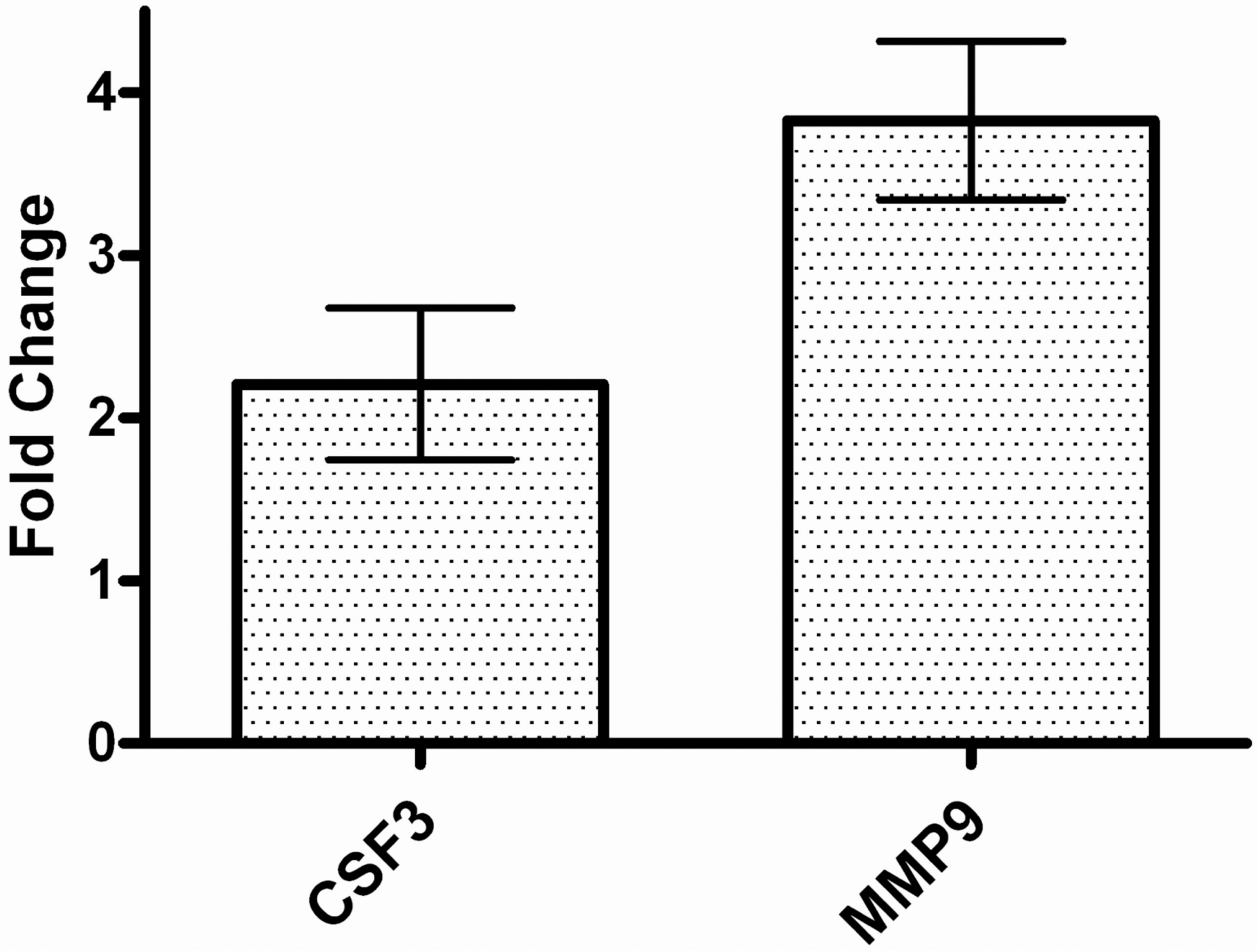

Figure 3.

ELISA validation of microarray results. Equivalent numbers of cells (4×10^6/well) were stimulated with LPS (1 μg/mL) in the absence or presence of 35 μM HNE for 24 h. CSF3 (colony stimulating factor 3 (granulocyte)) and MMP-9 (matrix metalloproteinase 9) released into the culture medium were analyzed by ELISA. Fold changes (HNE-treated stimulated cells relative to stimulated controls) are shown ($\bar{X} \pm$ SD for triplicate measurements, representative of three independent experiments).

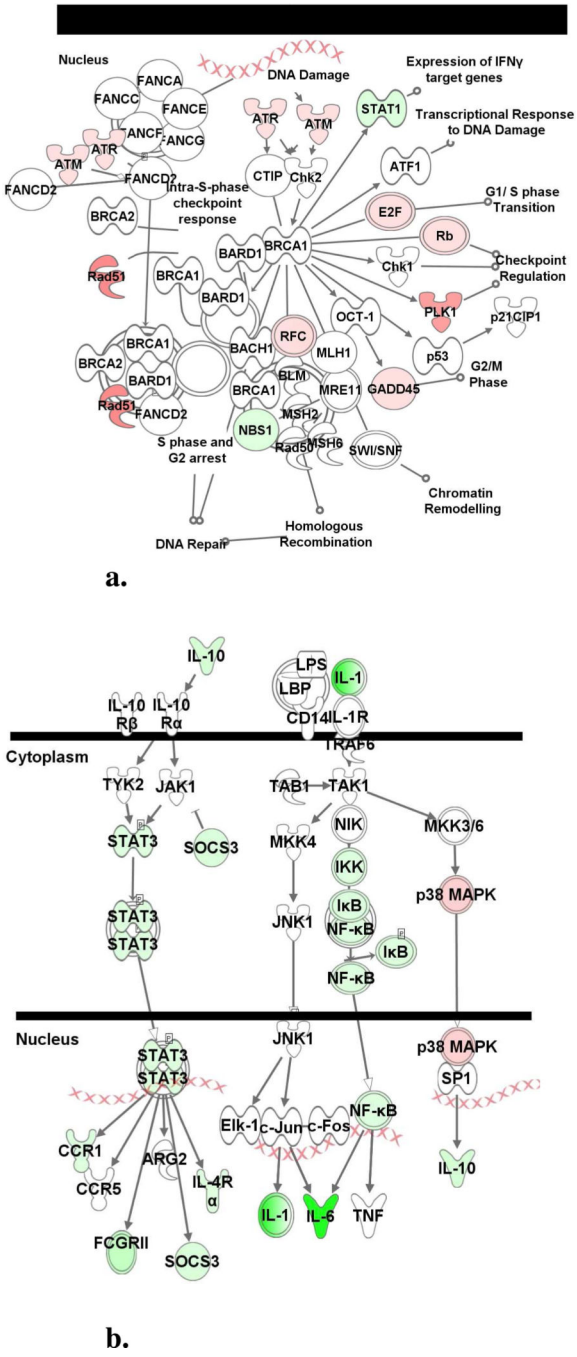

Figure 4.

Ingenuity canonical pathway analysis. Differentially expressed genes were mapped to the Ingenuity Canonical Pathway library to identify significantly altered canonical signaling pathways. (a) ‘IL-10 Signaling’ and (b) ‘Role of BRCA1 in DNA Damage Response’ were influenced by 35 μM HNE at 24 h and 6 h, respectively. Genes or gene products are represented as nodes and the intensity of the node color indicates the degree of up- (red) or down- (green) regulation.

Table 1

Taqman Gene Expression Assays Used for Quantitative Real-Time RT-PCR[a]

Treatment	Gene	Assay ID	Amplicon length
6 h BH, 6 h HNE	Csf2	Mm00438328_m1	71
6 h HNE	Ccl2	Mm00441242_m1	74
6 h HNE	Il1b	Mm00434228_m1	90
6 h HNE, 24 h BH	Il1a	Mm00439620_m1	68
6 h, 24 h HNE	Mmp9	Mm00442991_m1	76
6 h, 24 h HNE	Timp1	Mm00441818_m1	90
6 h, 24 h HNE	Csf3	Mm00438334_m1	106
24 h HNE	Ccl5	Mm01302428_m1	71
24 h HNE	Tnf	Mm00443258_m1	81
24 h HNE	Nfkbie	Mm00500796_m1	78
24 h HNE	Ikbke	Mm00444862_m1	66
24 h BH	Fos	Mm00487425_m1	59

[a]Each assay consists of two unlabeled PCR primers and a FAM™ dye-labeled TaqMan MGB (minor groove binder) probe.

Table 2

Functional analysis of BH and HNE datasets[a]

Biological Function	*p*-value[a]			
	BH		HNE	
	6 h	24 h	6 h	24 h
Amino Acid Metabolism			$< 10^{-04}$	2.03×10^{-04}
Carbohydrate Metabolism	5.54×10^{-04}			
Cell Cycle	5.54×10^{-04}	7.24×10^{-04}	$< 10^{-04}$	$< 10^{-04}$
Cell Death	2.41×10^{-04}		$< 10^{-04}$	$< 10^{-04}$
Cell Morphology		7.10×10^{-04}	$< 10^{-04}$	$< 10^{-04}$
Cell Signaling	5.61×10^{-04}		$< 10^{-04}$	
Cell-To-Cell Signaling and Interaction	$< 10^{-04}$		$< 10^{-04}$	$< 10^{-04}$
Cellular Assembly and Organization		1.61×10^{-04}	$< 10^{-04}$	$< 10^{-04}$
Cellular Compromise			$< 10^{-04}$	
Cellular Development	5.54×10^{-04}		$< 10^{-04}$	$< 10^{-04}$
Cellular Function and Maintenance	2.84×10^{-04}		$< 10^{-04}$	$< 10^{-04}$
Cellular Growth and Proliferation			$< 10^{-04}$	$< 10^{-04}$
Cellular Movement			$< 10^{-04}$	$< 10^{-04}$
DNA Replication, Recombination, and Repair			$< 10^{-04}$	$< 10^{-04}$
Free Radical Scavenging	5.54×10^{-04}			
Gene Expression			$< 10^{-04}$	$< 10^{-04}$
Lipid Metabolism	5.54×10^{-04}			
Molecular Transport	5.54×10^{-04}		$< 10^{-04}$	
Post-Translational Modification		6.25×10^{-04}	$< 10^{-04}$	$< 10^{-04}$
Small Molecule Biochemistry	5.54×10^{-04}		$< 10^{-04}$	2.03×10^{-04}
Vitamin and Mineral Metabolism			$< 10^{-04}$	

[a]Ingenuity Pathway Analysis uses a right-tailed Fisher Exact Test to calculate *p*-values. Significance values for each dataset indicate the probability that the association between the genes and the given molecular and cellular functions are due to random chance.

Table 3

Select Gene Expression Changes Mediated by HNE[a]

	Gene Symbol	Description	Fold Change		MGI Gene ID
			6 h	24 h	
Cell Cycle	Atm	ataxia telangiectasia mutated homolog (human)		1.9	107202
	Atr	Ataxia telangiectasia and rad3 related		3.8	108028
	Bub1	budding uninhibited by benzimidazoles 1 homolog (S. cere	−2.7		1100510
	Bub1b	budding uninhibited by benzimidazoles 1 homolog, beta (S.	−2.8		1333889
	Ccna2	cyclin A2	−5.1		108069
	Ccnb1	cyclin B1	−5.2		88302
	Ccnd1	cyclin D1		1.9	88313
	Ccnf	cyclin F	−4.1		102551
	Ccng2	cyclin G2	−2.9		1095734
	Ccr1	chemokine (C-C motif) receptor 1	−3.1		104618
	Cdc20	cell division cycle 20 homolog (S. cerevisiae)	−2.3		1859866
	Cdc25a	cell division cycle 25 homolog A (S. pombe)	−1.9		103198
	Cdc25c	cell division cycle 25 homolog C (S. pombe)	−3.5		88350
	Cdk6	cyclin-dependent kinase 6		1.9	1277162
	Chek1	checkpoint kinase 1 homolog (S. pombe)	−2.3		1202065
	Dbf4	DBF4 homolog (S. cerevisiae)	−2.0		1351328
	E2f2	E2F transcription factor 2		2.0	1096341
	Fen1	flap structure specific endonuclease 1		2.5	102779
	Gadd45a	growth arrest and DNA-damage-inducible 45 alpha		2.5	107799
	Mki67	antigen identified by monoclonal antibody Ki 67	−4.0		106035
	Msh5	mutS homolog 5 (E. coli)		6.2	1329021
	Mutyh	mutY homolog (E. coli)		3.1	1917853
	Mxd1	MAX dimerization protein 1	−4.7		96908
	Ndc80	NDC80 homolog, kinetochore complex component (S. cerevisia	−2.4		1914302

	Gene Symbol	Description	Fold Change		MGI Gene ID
			6 h	24 h	
	Pa2g4	proliferation-associated 2G4		2.3	894684
	Pcna	proliferating cell nuclear antigen		2.3	97503
	Plk1	polo-like kinase 1 (Drosophila)	−8.6		97621
	Rad23a	RAD23a homolog (S. cerevisiae)		2.2	105126
	Rad51	RAD51 homolog (S. cerevisiae)		16.3	97890
	Rbl1	retinoblastoma-like 1 (p107)		2.7	103300
	Riok3	RIO kinase 3	1.9		1914128
	Sass6	spindle assembly 6 homolog (C. elegans)	−2.4	−4.6	1920026
	Suv39h1	suppressor of variegation 3–9 homolog 1 (Drosophila)		2.4	1099440
	Tgfb	transforming growth factor, beta 1		2.0	98725
	Xaf1	XIAP associated factor 1	−2.1	−87.4	3772572
	Zwilch	Zwilch, kinetochore associated, homolog (Drosophila)	−2.3		1915264
Cell Signaling	Fcgr1a	Fc fragment of IgG, high affinity Ia, receptor (CD64)	−4.4	−13.6	95498
	Fcgr2b	Fc fragment of IgG, low affinity IIb, receptor (CD32)	−7.7	−2.9	95499
Cellular Development	Cd83	CD83 molecule	−2.4	−2.4	1328316
	Ifi16	interferon, gamma-inducible protein 16	−4.1	−11.6	96429
	Irf7	interferon regulatory factor 7	−3.4	−51.3	1859212
	Mafb	v-maf musculoaponeurotic fibrosarcoma oncogene homolog B (avian)	−4.4	−2.2	104555
Dyserythropoiesis	Ccl5	chemokine (C-C motif) ligand 5		−22.5	98262
	Traf3	Tnf receptor-associated factor 3		−2.3	108041
	Tsc22d3	TSC22 domain family, member 3		−3.6	1196284
ECM degradation	Mmp9	matrix metalloproteinase 9	−4.0	5.3	97011
	Timp1	tissue inhibitor of metalloproteinase 1	−8.5	-	98752
Gene Expression	Axud1	AXIN1 up-regulated 1	−3.0	−1.8	2387989
	Batf2	basic leucine zipper transcription factor, ATF-like 2	−1.8	−3.1	1921731
	Ddx58	DEAD (Asp-Glu-Ala-Asp) box polypeptide 58	−2.4	−14.2	2442858
	Mx1	myxovirus (influenza virus) resistance 1, interferon-	−7.9	−43.4	97243

	Gene Symbol	Description	Fold Change		MGI Gene ID
			6 h	24 h	
		inducible protein p78 (mouse)			
	Pcgf5	polycomb group ring finger 5	−1.8	−2.1	1923505
	Phf11	PHD finger protein 11	−2.9	−13.7	1918441
	Sp100	SP100 nuclear antigen	−2.8	−4.4	109561
Glutathione Metabolism	G6pd2	glucose-6-phosphate dehydrogenase 2	1.8	2.0	105977
	G6pdx	glucose-6-phosphate dehydrogenase X-linked	2.1		105979
	Gclc	glutamate-cysteine ligase, catalytic subunit	8.6		104990
	Gclm	glutamate-cysteine ligase , modifier subunit	7.6		104995
	Gss	glutathione synthetase	2.4		95852
	Gsta1	glutathione S-transferase, alpha 1 (Ya)	7.2	30.7	1095417
	Gstp1	glutathione S-transferase, pi 1	1.8		95865
	Idh1	isocitrate dehydrogenase 1 (NADP+), soluble	3.3		96413
	Pgd	phosphogluconate dehydrogenase	2.4		97553
Immune Response	Adrb2	adrenergic, beta-2-, receptor, surface	4.1	2.2	87938
	C5r1	complement component 5, receptor 1		3.5	88232
	Casp4	caspase 4, apoptosis-related cysteine peptidase	−2.2	−2.4	107700
	Ccl17	chemokine (C-C motif) ligand 17		3.1	1329039
	Ccl2	chemokine (C-C motif) ligand 2	−44.8		98259
	Ccl22	chemokine (C-C motif) ligand 22	−12.3		1306779
	Ccl4	chemokine (C-C motif) ligand 4	−2.1		98261
	Ccl6	chemokine (C-C motif) ligand 6	−3.1		98263
	Ccl7	chemokine (C-C motif) ligand 7	−22.6	−2.3	99512
	Ccr1	chemokine (C-C motif) receptor 1	−3.1		104618
	Cd14	CD14 antigen		2.2	88318
	Cd300lf	CD300 antigen like family member F	−3.9		2442359
	Cd40	CD40 antigen	−4.3		88336
	Cd44	CD44 antigen	−2.6		88338
	Cd86	CD86 antigen	−1.8		101773

	Gene Symbol	Description	Fold Change		MGI Gene ID
			6 h	24 h	
	Cenpa	centromere protein A	−2.3		88375
	Cfb	complement factor B	−7.4		105975
	Clec12a	C-type lectin domain family 12, member a	−1.9		3040968
	Clec2d	C-type lectin domain family 2, member d	−4.1		2135589
	Clec4n	C-type lectin domain family 4, member n	−2.4		1861231
	Clec5a	C-type lectin domain family 5, member a	−1.8		1345151
	Csf2	colony stimulating factor 2 (granulocyte-macrophage)	−12.1		1339752
	Csf3	colony stimulating factor 3 (granulocyte)	−18.2	18.0	1339751
	Cxcl1	chemokine (C-X-C motif) ligand 1		2.7	108068
	Cxcl14	chemokine (C-X-C motif) ligand 14	−2.7		1888514
	Cxcr4	chemokine (C-X-C motif) receptor 4	2.5		109563
	Dcn	decorin		−4.0	94872
	Ercc1	excision repair cross-complementing rodent repair deficient	−1.8		95412
	F10	coagulation factor X		4.1	103107
	Fbxo5	F-box protein 5	−4.0		1914391
	Gbp1	guanylate binding protein 1	−3.1	−16.8	95666
	Gbp3	guanylate nucleotide binding protein 3	−3.7		1926263
	Gbp5	guanylate nucleotide binding protein 5	−5.9		2429943
	H28	histocompatibility 28	−6.3		95975
	Hdc	histidine decarboxylase	−8.8	−3.1	96062
	Icam1	intercellular adhesion molecule 1	1.8	7.5	96392
	Igf1	insulin-like growth factor 1		2.1	96432
	Il10	interleukin 10	−4.7		96537
	Il10ra	interleukin 10 receptor, alpha		3.7	96538
	Il13ra1	interleukin 13 receptor, alpha 1	−3.4		105052
	Il18	interleukin 18	−2.0		107936
	Il18rap	interleukin 18 receptor accessory protein	−2.8		1338888

	Gene Symbol	Description	Fold Change		MGI Gene ID
			6 h	24 h	
	Il1a	interleukin 1 alpha	−66.6		96542
	Il1b	interleukin 1 beta	−32.7		96543
	Il1f6	interleukin 1 family, member 6	−12.6		1859324
	Il1rl1	interleukin 1 receptor-like 1	−3.6		98427
	Il1rn	interleukin 1 receptor antagonist	−6.8		96547
	Il27	interleukin 27	−6.4		2384409
	Il4ra	interleukin 4 receptor, alpha	−2.9		105367
	Il6	interleukin 6	−43.3	−11.2	96559
	Isg20	interferon stimulated exonuclease gene 20kDa	−3.1	−7.6	1928895
	Ltb	lymphotoxin B	−1.9		104796
	Nlrc4	NLR family, CARD domain containing 4	2.3	2.7	3036243
	Oasl2	2′–5′ oligoadenylate synthetase-like 2	−5.1		1344390
	Pgdfb	platelet derived growth factor, B polypeptide		3.2	97528
	Pla2g7	phospholipase A2, group VII (platelet-activating factor acetylhydrolase, plasma)	3.1	10.7	1351327
	Pou2f2	POU domain, class 2, transcription factor 2	−1.9		101897
	Rsad2	radical S-adenosyl methionine domain containing 2	−4.4		1929628
	Tnf	tumor necrosis factor		8.7	104798
	Traf3ip2	Traf3 interacting protein 2	−1.8		2143599
	Ube2L6	ubiquitin-conjugating enzyme E2L 6	−1.8	−2.3	1914500
	Vegfa	vascular endothelial growth factor A		−2.4	103178
Interferon-associated Signaling or Regulation	H2-Bf	histocompatibility 2, complement component factor B		−51.0	105975
	H2-DMb2	histocompatibility 2, class II, locus Mb2		−5.1	95923
	H2-Q1	histocompatibility 2, Q region locus 1		−3.2	95928
	H2-Q5	histocompatibility 2, Q region locus 5		−2.1	95934
	H2-T23	histocompatibility 2, T region locus 23		−9.4	95957
	H2-T9/H2-T22	histocompatibility 2, T region locus 9;histocompatibility 2, T region locus 22		−5.2	95965

	Gene Symbol	Description	Fold Change 6 h	Fold Change 24 h	MGI Gene ID
	Ifi202b	interferon activated gene 202B	−3.8		1347083
	Ifi203	interferon activated gene 203	−3.7		96428
	Ifi204	interferon activated gene 204	−3.7		96429
	Ifi205	interferon activated gene 205	−4.3		101847
	Ifi47	interferon gamma inducible protein 47	−3.0		99448
	Ifih1	interferon induced with helicase C domain 1	−2.0		1918836
	Ifit1	interferon-induced protein with tetratricopeptide repeats 1	−3.6		99450
	Ifit2	interferon-induced protein with tetratricopeptide repeats 2	−6.3		99449
	Ifit3	interferon-induced protein with tetratricopeptide repeats 3	−3.3		1101055
	Irf8	interferon regulatory factor 8	−2.6		96395
	Jak2	Janus kinase 2	−1.7		96629
	Mx2	myxovirus (influenza virus) resistance 2	−7.3		97244
	Oas1a	2’–5’ oligoadenylate synthetase 1A	−2.0		2180860
	Ptges	prostaglandin E synthase		4.7	1927593
	Stat1	signal transducer and activator of transcription 1	−2.2	−10.8	103063
	Stat3	signal transducer and activator of transcription 3	−2.1		103038
	Stat5a	signal transducer and activator of transcription 5A	−2.1		103036
Metabolic Process	Adh7	alcohol dehydrogenase 7 (class IV), mu or sigma polypeptide	8.0	2.3	87926
	Hbp1	high mobility group box transcription factor 1	2.9		894659
	Mov10	Mov10, Moloney leukemia virus 10, homolog (mouse)	−2.2	−2.5	97054
	Oas3	2'–5'-oligoadenylate synthetase 3, 100kDa	−2.4	−8.3	2180850
	Parp12	poly (ADP-ribose) polymerase family, member 12	−2.1	−4.9	2143990
	Serpinb1b	serine (or cysteine) peptidase inhibitor, clade B, member 1b	2.8	4.3	2445361
	Tiparp	TCDD-inducible poly(ADP-ribose) polymerase	−1.8	−2.9	2159210
NF-kB signaling	Ikbke	inhibitor of kappaB kinase epsilon		3.2	1929612

	Gene Symbol	Description	Fold Change		MGI Gene ID
			6 h	24 h	
	Nfkbia	nuclear factor of kappa light chain gene enhancer in B-cells inhibitor, alpha		1.8	104741
	Nfkbie	nuclear factor of kappa light polypeptide gene enhancer in B-cells inhibitor, epsilon		3.6	1194908
Oxidative Stress Response	Abcc1	ATP-binding cassette, sub-family C (CFTR	2.1		102676
	Akr1a4	aldo-keto reductase family 1, member A4 (aldehyde reducta	1.8		1929955
	Aox1	aldehyde oxidase 1	2.2		88035
	Cat	catalase	3.1		88271
	Dnajb4	DnaJ (Hsp40) homolog, subfamily B, member 4	5.3		1914285
	Ephx1	epoxide hydrolase 1, microsomal	2.0	3.2	95405
	Hmox1	heme oxygenase (decycling) 1	6.0		96163
	Mapk14	mitogen-activated protein kinase 14	2.0		1346865
	Pik3cb	phosphatidylinositol 3-kinase, catalytic, beta polypeptid	2.3		1922019
	Prdx1	peroxiredoxin 1	2.9	3.1	99523
	Raf1	v-raf-leukemia viral oncogene 1	2.2		97847
	Sod2	superoxide dismutase 2, mitochondrial		1.7	98352
	Sqstm1	sequestosome 1	3.1		107931
	Txnrd1	thioredoxin reductase 1	2.1		1354175
	Xdh	xanthine dehydrogenase	2.0		98973
Signal Transduction	Fcrl1	Fc receptor-like 1	3.5	3.9	2442862
	Lyn	Yamaguchi sarcoma viral (v-yes-1) oncogene homolog	−1.9		96892
	Rasgrp3	RAS guanyl releasing protein 3 (calcium and DAG-regulated)	3.9	4.4	3028579
	Rit1	Ras-like without CAAX 1	2.1		108053
Small Molecule Biochemistry	Cp	ceruloplasmin (ferroxidase)	−7.7	−6.0	88476
	Slc7A2	solute carrier family 7 (cationic amino acid transporter, y+ system), member 2	−5.2	−5.2	99828

	Gene Symbol	Description	Fold Change		MGI Gene ID
			6 h	24 h	
Cell Structure	Gsn	gelsolin		2.5	95851
	Stmn1	stathmin 1		10.8	96739
	Tuba4	tubulin, alpha 4		2.5	1095410
Ubiquitin-Proteasome Pathway	Fbxl17	F-box and leucine-rich repeat protein 17	1.8		1354704
	Fbxl20	F-box and leucine-rich repeat protein 20	2.1		1919444
	Fbxo22	F-box only protein 22		3.0	1926014
	Fbxo30	F-box protein 30	2.0		1919115
	Fbxo31	F-box protein 31	1.8		1354708
	Herc3	hect domain and RLD 3	2.3		1921248
	Map1lc3b	microtubule-associated protein 1 light chain 3 beta	2.0		1914693
	Psmc3ip	proteasome (prosome, macropain) 26S subunit, ATPase 3, interacting protein		6.4	1098610
	Psmd12	proteasome (prosome, macropain) 26S subunit, non-ATPase, 12		2.0	1914247
	Rnf128	ring finger protein 128	4.2		1914139
	Rnf167	ring finger protein 167	1.9		1917760
	Ube2d3	ubiquitin-conjugating enzyme E2D 3 (UBC4/5		2.4	1913355
	Ube2i	ubiquitin-conjugating enzyme E2I		3.0	107365
	Ube2t	ubiquitin-conjugating		7.1	1914446
	Ube4b	ubiquitination factor E4B, UFD2 homolog (S.	1.8		1927086
	Uchl1	ubiquitin carboxy-terminal hydrolase L1		4.4	103149
	Usp18	ubiquitin specific protease 18		−224.6	1344364
Other	Arrdc3	arrestin domain containing 3	7.0		2145242
	Bcl2l11	BCL2-like 11 (apoptosis facilitator)	2.0		1197519
	Epsti1	epithelial stromal interaction 1 (breast)	−2.1	−10.6	1915168
	Gabarapl1	gamma-aminobutyric acid (GABA(A)) receptor-	2.8		1914980
	Id1	inhibitor of DNA binding 1	−2.0		96396
	Ier3	immediate early response 3	−2.0		104814
	Ifi203	interferon activated gene 203	−3.7	−5.2	96428

	Gene Symbol	Description	Fold Change		MGI Gene ID
			6 h	24 h	
	Klhl6	kelch-like 6 (Drosophila)	−1.9	−3.8	2686922
	Map1d	methionine aminopeptidase 1D	1.8	1.9	1913809
	Ms4A6D	membrane-spanning 4-domains, subfamily A,	−2.3	−3.9	1916024
	Top2a	topoisomerase (DNA) II alpha	13.2		98790
	Trim30	tripartite motif-containing 30	−7.2	−31.8	98178
	Uvrag	UV radiation resistance associated gene	−1.9	−1.8	1925860
	Zak	sterile alpha motif and leucine zipper containing	−1.9	−4.0	2443258
	Zbp1	Z-DNA binding protein 1	−5.7	−69.4	1927449
	Zbtb20	zinc finger and BTB domain containing 20	3.6		1929213
	Zfp36	zinc finger protein 36	−1.9		99180

[a]Genes altered ≥1.8-fold ($p \leq 0.01$) up or down in LPS stimulated HNE-treated cells relative to LPS stimulated cells. Fold changes (FC) represent the average of three independent biological experiments.

Table 4

Select Gene Expression Changes Mediated by BH[a]

	Gene Symbol	Description	Fold Change		MGI Gene ID
			6 h	24 h	
Interferon-associated Signaling or Regulation	H2-Ab1	histocompatibility 2, class II antigen A, beta 1		−1.8	103070
	H2-Q1	histocompatibility 2, Q region locus		−4.8	95928
Immune Response	Ccl2	chemokine (C-C motif) ligand 2		2.2	98259
	Ccl6	chemokine (C-C motif) ligand 6		5.4	98263
	Cd2	CD2 antigen		102.4	88320
	Csf2	colony stimulating factor 2 (granulocyte-macrophage)	−12.1		1339752
	Cxcl2	chemokine (C-X-C motif) ligand 2		1.9	1340094
	Ereg	epiregulin		13.2	107508
	Fos	FBJ osteosarcoma oncogene		−3.6	95574
	Il1a	interleukin 1 alpha		6.0	96542
	Il20	interleukin 20		2.4	1890473
Oxidative Stress Response	Hmox1	heme oxygenase (decycling) 1	6.0		96163
Cell Structure	Pstpip2	proline-serine-threonine phosphatase interacting protein 2		6.1	1335088
	Tuba4	tubulin, alpha 4		1.9	1095410

[a]Genes altered ≥1.8-fold ($p \leq 0.01$) up or down in LPS stimulated BH-treated cells relative to LPS stimulated cells. Fold changes (FC) represent the average of three independent biological experiments.